



Transit time scattering of energetic electrons due to equatorially confined magnetosonic waves

J. Bortnik¹ and R. M. Thorne¹

Received 15 January 2010; revised 10 February 2010; accepted 4 March 2010; published 15 July 2010.

[1] Recent analysis using quasilinear theory (QLT) has shown that magnetosonic (MS) waves are able to accelerate electrons to relativistic energies on fast time scales (~ 1 day). However, the large obliquity of the wave and typical equatorial confinement of the MS wave power create conditions that bring into question the fundamental applicability of QLT to this problem. In this paper, a test particle code is used to model the interaction of energetic electrons with fast MS waves, to test the results of QLT analysis, and to investigate any potential nonlinear effects. It is found that in the expected Landau-resonant region, test particle results show good agreement with QLT, but outside this region, the spatial confinement of the low-frequency waves introduces a new source of scattering which we call “transit time diffusion.” Although this mechanism is weaker than resonant scattering, it is nevertheless able to interfere with the Landau resonance to create nulls in the energy-pitch angle diffusion map, and the scattering persists even when resonant diffusion is completely removed.

Citation: Bortnik, J., and R. M. Thorne (2010), Transit time scattering of energetic electrons due to equatorially confined magnetosonic waves, *J. Geophys. Res.*, 115, A07213, doi:10.1029/2010JA015283.

1. Introduction

[2] Fast magnetosonic (MS) waves have recently become the focus of renewed interest because of their potential to accelerate radiation belt electrons on a time scale of ~ 1 day, which is comparable to the time scale of acceleration by other known leading mechanisms such as chorus [Horne *et al.*, 2007]. In contrast to the earliest studies of MS wave scattering which focused on the violation of the second adiabatic invariant through bounce-resonant interactions [Roberts and Schulz, 1968], Horne *et al.* demonstrated that the first adiabatic invariant of the particles can be efficiently violated through Landau resonant interactions with the highly oblique MS wave.

[3] MS waves are primarily confined within $\sim 2^\circ$ – 3° of the geomagnetic equator [Russell *et al.*, 1970; Santolik *et al.*, 2002; Nemeč *et al.*, 2005, 2006], and occur both inside and outside the plasmopause in the range $L \sim 2$ – 7 [Gurnett, 1976; Perraut *et al.*, 1982; Laakso *et al.*, 1990], preferentially in the postnoon or dusk sector [Green *et al.*, 2005; Pokhotelov *et al.*, 2008]. Typical observations show that MS waves occur as a series of narrow tones, spaced at multiples of the proton gyrofrequency (f_{ci}), in the range between f_{ci} and the lower hybrid resonance frequency (f_{LHR}). These observations led early workers to the idea that MS waves derive their energy from a resonant interaction with a highly anisotropic “ring”

distribution of energetic protons [e.g., Gurnett, 1976; Perraut *et al.*, 1982; Boardsen *et al.*, 1992; Horne *et al.*, 2000; Meredith *et al.*, 2008]. Moreover, MS waves were shown to occur with an unusually high probability ($\sim 60\%$) and shown to have the most intense wave electric field compared with all other natural emissions, in the range of CLUSTER equatorial passes ($L \sim 4$ – 5) [Santolik *et al.*, 2004].

[4] A defining characteristic of MS waves is the near-perpendicular angle ($\psi \sim 89^\circ$) formed between its \mathbf{k} vector and the static magnetic field \mathbf{B}_0 [e.g., Russell *et al.*, 1970], as illustrated schematically in Figure 1a. This topology results in a propagation path that “snakes” about the geomagnetic equator (Figure 1a, red curve), but remains essentially perpendicular to \mathbf{B}_0 , and leads to various effects such as the equatorial confinement of the wave power described above (gray region in Figure 1a, and Figure 1b), an extended resonance with the (also equatorially confined) proton ring distribution, potential azimuthal guiding by the plasmopause [Kasahara *et al.*, 1994], and some radial translation which can lead to a nonlocal f_{ci} spacing between the MS harmonic lines [Santolik *et al.*, 2002]. In addition, since $k_\perp \gg k_\parallel$, the component of wavelength parallel to \mathbf{B}_0 (λ_\parallel) can often exceed the spatial confinement of the waves. For example, using the parameters described in section 2 that are used in the present paper and taken directly from Horne *et al.* [2007], $k_\parallel \sim 2.17 \times 10^{-6} \text{ m}^{-1}$, so that $\lambda_\parallel = 2,900 \text{ km}$ which translates to a latitudinal extent of $\sim 5.8^\circ$ at $L = 4.5$. Consequently, an energetic electron traversing the MS wavefield experiences only a fraction of a wavelength. This raises questions concerning the applicability of quasilinear theory to the problem of MS wave scattering [Horne *et al.*, 2007; Kennel and Engelmann, 1966], and the large amplitude of MS waves in relation to the

¹Department of Atmospheric and Oceanic Sciences, University of California, Los Angeles, California, USA.

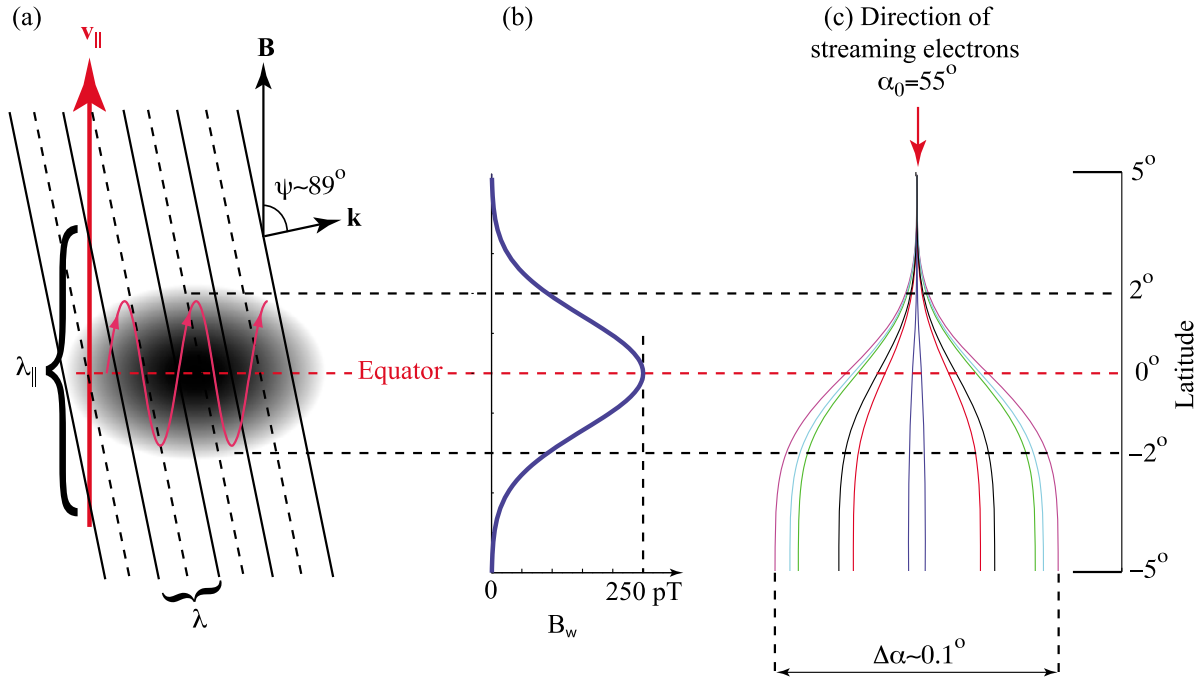


Figure 1. Schematic of magnetosonic wave geometry showing (a) obliquity, ray trajectory “snaking” about the equator, equatorial confinement, and resultant extent of λ_{\parallel} , (b) distribution of magnetic amplitude as a function of latitude, and (c) pitch angle scattering of $E_0 = 300$ keV, $\alpha_0 = 55^\circ$ electrons, corresponding to R_2 in Figure 3.

low background magnetic field inhomogeneity [e.g., *Omura et al.*, 2008; *Bortnik et al.*, 2008; *Albert and Bortnik*, 2009] requires an assessment of whether nonlinear processes might affect the electron dynamics. To address these questions, the interaction between a MS wave and energetic electrons is modeled in the present paper using a nonlinear, relativistic, oblique test particle code. The numerical simulation and relevant equations are described in section 2, the results of a large number of modeled interactions are described and discussed in sections 3 and 4, and the conclusions are presented in section 5.

2. Test Particle Simulation

2.1. Equations of Motion

[5] The dynamics of an electron, with rest mass m_e and charge q_e moving in an electromagnetic field are described by the Lorentz force equation:

$$\frac{d\mathbf{p}}{dt} = q_e \left\{ \mathbf{E}^w + \frac{\mathbf{p}}{m_e \gamma} \times [\mathbf{B}^w + \mathbf{B}_0(\lambda)] \right\} \quad (1)$$

where $\mathbf{p} = \gamma m_e \mathbf{v}$ is the electron momentum, $\gamma = (1 - v^2/c^2)^{-1/2}$, $\mathbf{v} = d\mathbf{r}/dt$ is the particle velocity vector, and the total field has been explicitly separated into the static geomagnetic field \mathbf{B}_0 , and the wave components \mathbf{E}^w , \mathbf{B}^w , all of which are functions of distance (or equivalently, latitude) along the field line. Although (1) can be integrated directly, it is often more instructive and computationally economical to separate the interaction into an infinite sum of resonances, and gyro-average the equations so that numerical integration

can proceed on time scales comparable to the gyroperiod. Following a procedure similar to that of *Bell* [1984] (used previously by various authors [e.g., *Jasna et al.*, 1992; *Lauben et al.*, 2001; *Bortnik et al.*, 2006]) we write the oblique whistler wave components as:

$$\mathbf{E}^w = -\hat{x}E_x^w \sin \Phi + \hat{y}E_y^w \cos \Phi - \hat{z}E_z^w \sin \Phi \quad (2)$$

$$\mathbf{B}^w = \hat{x}B_x^w \cos \Phi + \hat{y}B_y^w \sin \Phi - \hat{z}B_z^w \cos \Phi \quad (3)$$

where $\Phi(\mathbf{r}) = \int \omega dt - \int \mathbf{k} \cdot d\mathbf{r}$ is the wave phase. Since the gyroradius of resonant energetic electrons is typically much smaller than the spatial scales of variation of \mathbf{B}_0 at the L shells of interest, we neglect the asymmetrical variation of \mathbf{B}_0 in the perpendicular direction (which typically lead to magnetic drift motion), i.e., $\mathbf{B}_0(x, y, z) = \mathbf{B}_{0z}(0, 0, z) \equiv \mathbf{B}_0(z)$.

[6] Since the whistler mode wavefield (which connects to the magnetosonic mode along the same dispersion curve) is naturally elliptically polarized in the plasma, we transform to a rotating coordinate system and decompose the wave into two circularly polarized components with opposite senses of rotation, i.e.,

$$\mathbf{B}_R^w = \frac{B_x^w + B_y^w}{2} [\hat{x} \cos \Phi + \hat{y} \sin \Phi] \quad (4)$$

$$\mathbf{B}_L^w = \frac{B_x^w - B_y^w}{2} [\hat{x} \cos \Phi - \hat{y} \sin \Phi] \quad (5)$$

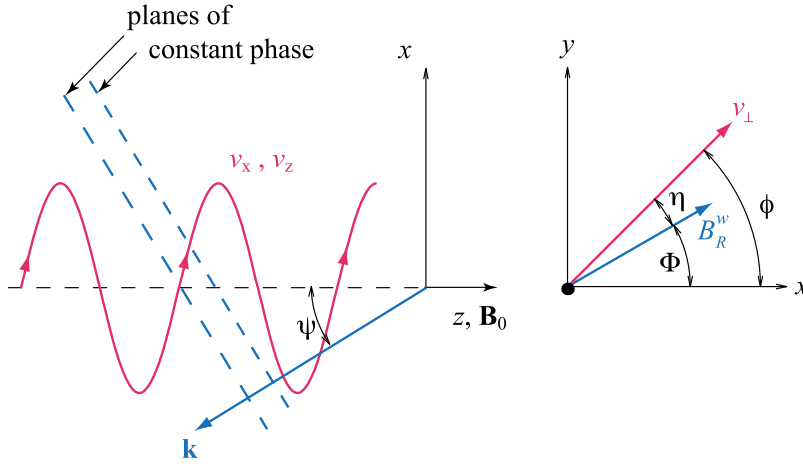


Figure 2. Interaction geometry between an energetic electron (red) and an obliquely propagating whistler wave (blue), showing the wave normal angle ψ , and the angle η between v_{\perp} and B_R^w where v_{\perp} is the velocity component of the electron perpendicular to \mathbf{B}_0 and B_R^w is the right circularly polarized wave component.

[7] Using the above decomposition together with (1) and averaging over a gyroperiod, we obtain the relativistic gyro-averaged equations of motion for a general harmonic resonance m :

$$\frac{dp_{\parallel}}{dt} = \omega_{\tau m}^2 m_e k_{\parallel}^{-1} \sin \eta - \frac{1}{m_e \gamma} \frac{p_{\perp}^2}{2\omega_{ce}} \frac{\partial \omega_{ce}}{\partial z} \quad (6)$$

$$\begin{aligned} \frac{dp_{\perp}}{dt} = & - \left[\omega_1 \left(\frac{p_{\parallel}}{\gamma} + m_e R_1 \right) J_{m-1}(\beta) - \dots \right. \\ & \left. \omega_2 \left(\frac{p_{\parallel}}{\gamma} - m_e R_2 \right) J_{m+1}(\beta) \right] \sin \eta + \dots \\ & \frac{1}{m_e \gamma} \frac{p_{\parallel} p_{\perp}}{2\omega_{ce}} \frac{\partial \omega_{ce}}{\partial z} \end{aligned} \quad (7)$$

$$\frac{d\eta}{dt} = \frac{m\omega_{ce}}{\gamma} - \omega - k_{\parallel} \frac{p_{\parallel}}{m_e \gamma} \quad (8)$$

where η is defined as the angle between B_R^w and v_{\perp} and is shown in Figure 2, ω is the whistler wave radial frequency, and $\omega_{ce} = -q_e B_0 / m_e = e B_0 / m_e$ is the electron gyrofrequency. J_i are Bessel functions of the first kind, order i , whose argument is proportional to the particle gyroradius in terms of perpendicular wavelenghts, and represents the asymmetry of the wavefield as experienced by the gyrating particle. The remaining equations are:

$$\beta = \frac{k_{\perp} p_{\perp}}{m_e \gamma \omega_{ce}} \quad (9)$$

$$k_{\parallel} = k \cos \psi = (\omega \mu / c) \cos \psi; \quad k_{\perp} = k \sin \psi \quad (10)$$

$$\omega_{\tau m}^2 = (-1)^{m-1} \omega_{\tau 0}^2 [J_{m-1}(\beta) - \alpha_1 J_{m+1}(\beta) + \gamma \alpha_2 J_m(\beta)] \quad (11)$$

$$\omega_{\tau 0}^2 = \frac{\omega_1 k_{\parallel} p_{\perp}}{\gamma m_e} \quad (12)$$

$$\omega_1 = \frac{e}{2m_e} (B_x^w + B_y^w); \quad \omega_2 = \frac{e}{2m_e} (B_x^w - B_y^w) \quad (13)$$

$$\alpha_1 = \frac{\omega_2}{\omega_1}; \quad \alpha_2 = \frac{e E_z^w}{\omega_1 p_{\perp}} \quad (14)$$

$$R_1 = \frac{E_x^w + E_y^w}{B_x^w + B_y^w}; \quad R_2 = \frac{E_x^w - E_y^w}{B_x^w - B_y^w} \quad (15)$$

where μ is the refractive index and $\omega_{\tau 0}$ is the trapping frequency. A more complete description of the various terms can be found in *Bell* [1984]. To close the set of equations, we note that the wave electric and magnetic field components are not independent, but are related through the physics of the propagation mode [e.g., *Stix*, 1992]. Following *Bell* [1984], *Jasna et al.* [1992] and *Lauben et al.* [2001], we relate the Poynting flux of the wave $\mathbf{S}^w = (1/2) \Re \{ \mathbf{E}^w \times \mathbf{H}^w \}$, as well as all other wave components to the single reference component B_y^w as:

$$\left| B_y^w \right|^2 = \frac{2\mu_0 \rho_2^2 X^2 \mu \cos \psi |\mathbf{S}^w|}{c \sqrt{(\tan \psi - \rho_1 \rho_2 X)^2 + (1 + \rho_2^2 X)^2}} \quad (16)$$

where

$$X = \frac{P}{P - \mu^2 \sin^2 \psi} \quad (17)$$

$$\rho_1 = \frac{E_z^w}{E_y^w} = \frac{(\mu^2 - S) \mu^2 \sin \psi \cos \psi}{D(\mu^2 \sin^2 \psi - P)} \quad (18)$$

$$\rho_2 = \frac{E_x^w}{E_y^w} = \frac{\mu^2 - S}{D} \quad (19)$$

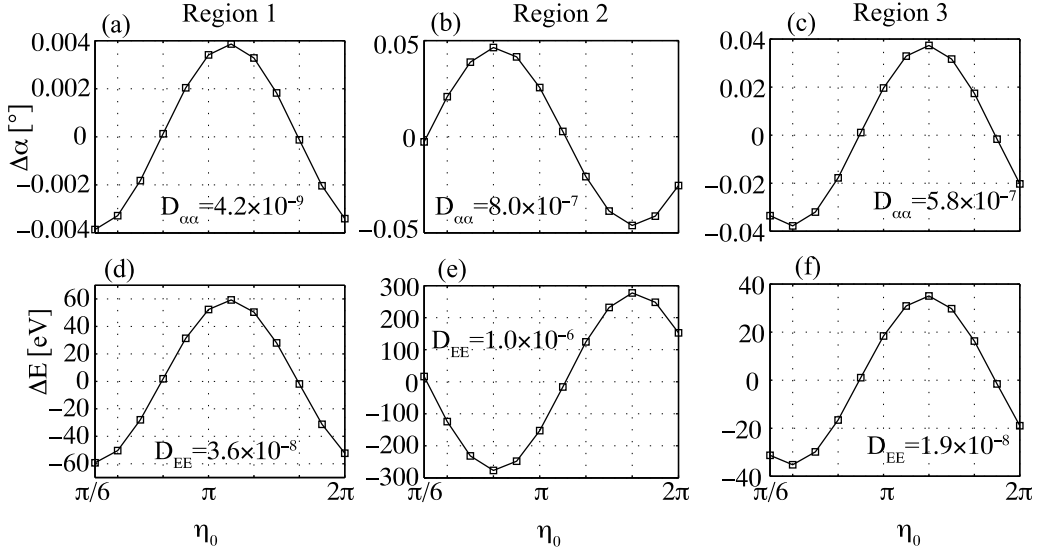


Figure 3. Pitch angle and energy changes ($\Delta\alpha$, ΔE) of 300 keV electrons in 3 regions corresponding to those in Figures 4 and 5: (a, d) Region 1, $\alpha_0 = 20^\circ$; (b, e) Region 2, $\alpha_0 = 55^\circ$; and (c, f) Region 3, $\alpha_0 = 78^\circ$.

and

$$\begin{aligned}
 \frac{E_x^w}{B_y^w} &= \frac{c(P - \mu^2 \sin^2 \psi)}{P\mu \cos \psi}, \\
 \frac{E_y^w}{B_y^w} &= \frac{Dc(P - \mu^2 \sin^2 \psi)}{P\mu \cos \psi(S - \mu^2)}, \\
 \frac{E_z^w}{B_y^w} &= \frac{-c\mu \sin \psi}{P}, \\
 \frac{B_x^w}{B_y^w} &= \frac{-D(P - \mu^2 \sin^2 \psi)}{P(S - \mu^2)}, \\
 \frac{B_z^w}{B_y^w} &= \frac{D \sin \psi (P - \mu^2 \sin^2 \psi)}{P \cos \psi (S - \mu^2)}
 \end{aligned} \quad (20)$$

where c is the speed of light, $\mu_0 = 4\pi \times 10^{-7}$ H/m is the permeability of free space, and all other symbols are as previously defined. We note that the ratios expressed in (20) relate the magnitudes of the wave components and are always taken to be positive in the present work.

[8] Equations (6)–(20) are solved by specifying the wave intensity (S^w or B_y^w) and wavenormal ψ as a function of latitude, together with the standard dipole expressions for the variation of B_0 , and its spatial derivative. A test particle is then selected with an initial energy (E_0), equatorial pitch angle (α_0), wave-particle phase (η_0), and starting location (L and λ_0). Given these parameters, the set of equations (6)–(8) can be numerically integrated using standard ordinary differential equation solvers (in our case, the Adams-Bashford-Moulton solver is used).

2.2. Simulation Parameters

[9] In order to model the interaction of energetic electrons with fast MS waves, the parameters used by *Horne et al.* [2007] are followed as closely as possible. Groups of 12 individual electrons, uniformly distributed in η_0 are launched from a latitude of $\lambda_0 \sim 5^\circ$ at $L = 4.5$, into a wave

packet having $\psi = 89^\circ$, $f = 33.3$ Hz, and an amplitude envelope $B^w = B_0^w \exp(-(\lambda/\lambda_w)^2)$, where the latitudinal width is taken to be $\lambda_w = 2^\circ$, and $B_0^w = 250$ pT (Figure 1b). The geomagnetic field is taken to be dipolar, and the plasma is assumed to be composed of electrons and ions, varying with latitude as $n_e = n_{e0} \cos^{-4} \lambda$, after *Denton et al.* [2002], with $n_{e0} = 10.3 \text{ cm}^{-3}$ such that $f_{pe}/f_{ce} = 3$ at $L = 4.5$. The wave normal ψ is taken to be always in the same direction, and does not vary with latitude or change sign across the equator. The equations of motion described above are integrated for all the test particles until they have completed a single traverse through the wave packet and have exited at $\lambda_f \sim -5^\circ$ (Figure 1c). At this point, the final equatorial pitch angle and energy of each particle is recorded and used in subsequent analyses.

[10] The above parameters were chosen to match those of *Horne et al.* [2007] as closely as possible, with the exception of the Gaussian spatial variation of wave power about the equator, which was introduced to eliminate any edge effects associated with the step-like increase in wave power at $\lambda = \pm 3^\circ$. To keep the total wave power traversed by the electron roughly similar, B_0^w was increased from 218 pT [*Horne et al.*, 2007] to 250 pT. Since the test particle approach used presently is inherently monochromatic, whereas the quasilinear formulation is wideband, any comparison should be treated as only approximate.

3. Results

[11] Figure 3 shows three examples of pitch angle and energy scattering for a group of 12 electrons having an initial energy of $E_0 = 300$ keV, and initial equatorial pitch angles of $\alpha_0 = 20^\circ$ (Figures 3a and 3d), $\alpha_0 = 55^\circ$ (Figures 3b and 3e), and $\alpha_0 = 78^\circ$ (Figures 3c and 3f). The interaction is only evaluated for $m = 0$ (Landau resonance), since the normal cyclotron resonance ($m = 1$) energy is very high >35 MeV, and beyond the energies of interest of the present study. Each particle is traced from its starting latitude ($\lambda_0 = 5^\circ$),

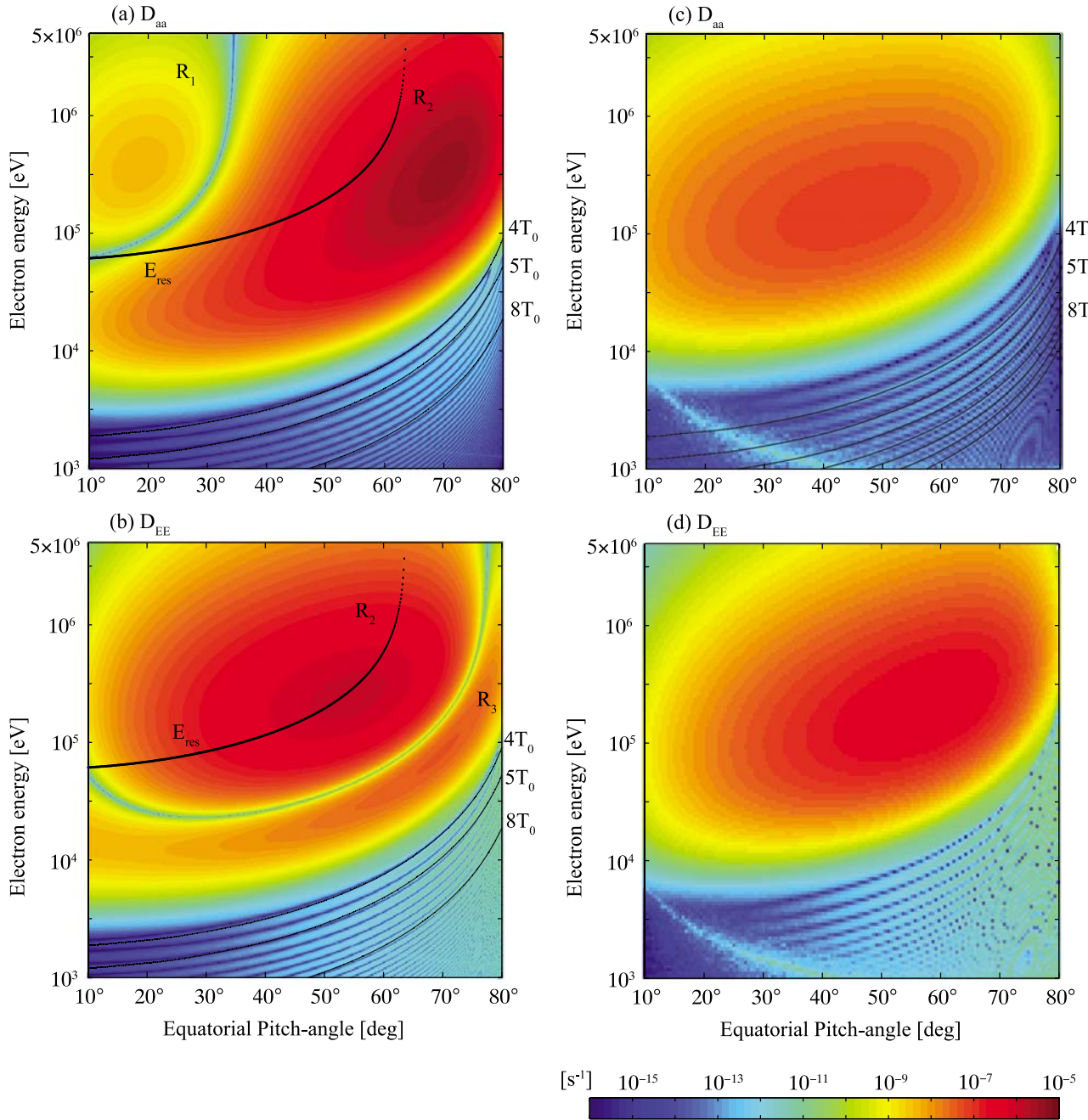


Figure 4. (a, c) Pitch angle and (b, d) energy diffusion coefficients as a function of energy and pitch angle. Figures 4a and 4b correspond to $\psi = 89^\circ$, and Figures 4c and 4d correspond to $\psi = 89.99^\circ$. E_{res} is the equatorial Landau resonant energy, the solid lines represent transit times corresponding to 4, 5, and 8 wave periods, and R_{1-3} correspond to Regions 1–3 (see text).

towards the Southern hemisphere, until it emerges from the wave packet at $\lambda_f = -5^\circ$, with a modified equatorial pitch angle λ_f [e.g., *Bortnik et al.*, 2008, Figures 1c and 1d]. The final wave-induced changes in pitch angle ($\Delta\alpha = \alpha_f - \alpha_0$), and energy ($\Delta E = E_f - E_0$) are shown in Figures 3a, 3b, and 3c and Figures 3d, 3e, and 3f, respectively.

[12] Despite the relatively large wave amplitude, and small inhomogeneity of the geomagnetic field which might be expected to lead to dramatic nonlinear effects [e.g., *Bortnik et al.*, 2008], the scattering in both $\Delta\alpha$ and ΔE varies

sinusoidally with η_0 , regardless of α_0 . This interaction is therefore linear, and would lead to diffusive scattering when multiple interactions are combined incoherently (i.e., as the particle bounces across the equator multiple times.). It is thus convenient to present our test particle scattering results in the form of diffusion coefficients, calculated as:

$$D_{\alpha\alpha} = \frac{1}{\tau_b} \sum_{n=1}^N \frac{(\Delta\alpha_i)^2}{N}, \quad D_{EE} = \frac{1}{\tau_b} \sum_{n=1}^N \frac{(\Delta E_i/E_0)^2}{N} \quad (21)$$

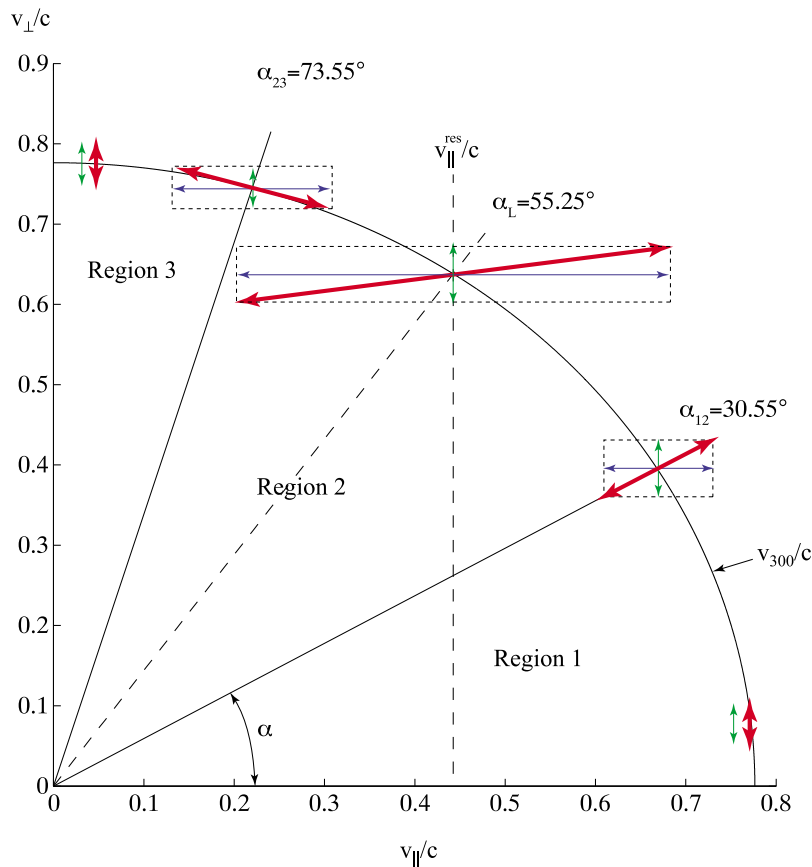


Figure 5. Velocity-space diagram showing the constant energy curve for a 300 keV electron ($v_{300}/c = 0.7765$), Regions 1–3 and associated separatrix angles. The green, blue, and red line segments represent the transit time, Landau, and resultant single-wave characteristics in the various regions.

where $N = 12$ particles distributed uniformly between 0 and 2π , and τ_b is the bounce time for the particle, approximated as $0.117L (c/v) (1 - 0.4635 \sin^{0.75} \alpha_{eq})$ [Walt, 1994, p. 44]. The equivalent diffusion coefficients (21) for the three cases shown in Figure 3 are indicated in each plot.

[13] Figure 4 shows $D_{\alpha\alpha}$ and D_{EE} for a range of energies from $E_0 = 1$ keV to 5 MeV, and pitch angles from $\alpha_0 = 10^\circ$ to 80° , calculated from an ensemble of test particle simulations, as outlined above. Both Figures 4a and 4b exhibit a broad maximum centered between ~ 100 keV and 1 MeV, at $\alpha_0 \sim 50^\circ$ – 70° , with values of $\sim 10^{-5} \text{ s}^{-1}$, that are primarily produced by the Landau resonance, and are comparable to the values obtained using quasilinear theory [Horne et al., 2007]. For reference, the Landau resonant energy (E_{res}) as a function of α_0 has been superposed on both Figures 4a and 4b, and it is apparent that the maximum in D_{EE} coincides with E_{res} for $\alpha_0 \sim 50^\circ$.

[14] However, in addition to the broad maximum introduced by the Landau resonance, additional scattering features are apparent in our simulations. For clarity we divide Figure 4 into 3 distinct regions: Region 1 (R_1) is a weak secondary maximum in $D_{\alpha\alpha}$, at $E \sim 400$ keV, $\alpha_0 < 30^\circ$; Region 2 (R_2) is the Landau resonance region, seen as the primary maximum in both $D_{\alpha\alpha}$ and D_{EE} near ~ 300 keV at $\alpha_0 \sim 50^\circ$ – 70° ; and Region 3 (R_3) is a secondary maximum in D_{EE} , visible primarily at large α_0 , and low E_0 . In addition

to these 3 dominant regions of scattering, $D_{\alpha\alpha}$ and D_{EE} also exhibit a weak series of striations at low E_0 . The presence of R_1 , R_3 , and the low E_0 striations can be attributed to the effects of the finite transit time of the electron as it traverses a spatially limited region of wave power, as discussed below.

4. Discussion

[15] The red line segments in Figure 5 indicate schematically the orientation of the resultant single-wave characteristic for 300 keV electron scattering at different pitch angles, i.e., the relationship between $\Delta\alpha_i$ and Δv_i for each test particle, as it is scattered by the wave. Landau resonant scattering leads to changes in v_{\parallel} as a consequence of the stationary parallel electric field E_{\parallel}^w in the rest frame of the resonant electron. Since the magnetosonic waves are highly oblique, the wave electric field is primarily perpendicular to \mathbf{B}_0 , and only a small component of the total wave electric field is involved in the Landau resonant energy transfer. The single-wave characteristic describing the Landau resonance in Region 2 is a horizontal line in velocity space (blue line segments), indicating that an electron scattered to lower α (i.e., $\Delta\alpha_i < 0$), will simultaneously increase in energy (i.e., $\Delta v_i > 0$), and vice versa, since only parallel momentum can be exchanged [e.g., Walker, 1993, p. 158]. The corresponding scattering curves are shown in Figures 3b and 3e,

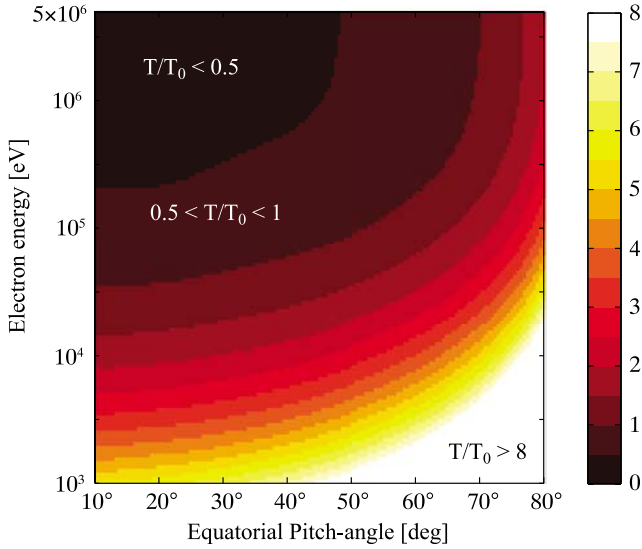


Figure 6. Time required for electrons to traverse the wave region expressed in wave periods (T_0), showing that the majority of energetic electrons interact with ~ 1 wave period or less.

which confirm that $\Delta\alpha_i\Delta E_i < 0$. At 300 keV, the resonant angle is $\alpha_L = 55.25^\circ$, corresponding to $v_{\parallel}^{\text{res}}/c = 0.4425$.

[16] Well away from α_L , the Landau resonance becomes weak, and scattering is provided by an additional process, which we refer to as “transit time diffusion.” In general, any nonresonant electron entering the magnetosonic wave packet experiences a force according to (1) from the first wave crest that it encounters, which scatters it in a particular direction. Traversing subsequent wave crests of opposite (alternating) polarity scatters the particle in alternating directions, which should average to zero, in the nonresonant case, for an infinite (or long) wave train. However, in Region 1, the particle experiences less than one half of a wave period during its traversal of the entire wave region ($\lambda \sim -3^\circ$ to 3°), and the particle experiences a net, albeit small, perturbation. The orientation of the magnetosonic wave is such that \mathbf{E}^w and \mathbf{B}^w are approximately perpendicular and parallel to \mathbf{B}_0 , respectively, which result in momentum exchange only in the perpendicular direction. The resulting single-wave characteristic for transit time diffusion is a vertical line in velocity-space (Regions 1 and 3 in Figure 5, indicated by the green line segments), implying that an electron scattered to lower α (i.e., $\Delta\alpha_i < 0$), would experience a decrease in energy (i.e., $\Delta v_i > 0$, $\Delta E_i > 0$). The corresponding scattering curves are shown in Figures 3a and 3d (Region 1) and Figures 3c and 3f (Region 3) for 300 keV electrons, indicating that the phasing of $\Delta\alpha_i$ and ΔE_i in Regions 1 and 3 is opposite to that of Region 2, and $\Delta\alpha_i\Delta E_i > 0$.

[17] The scattering in v_{\perp} associated with transit time diffusion leads to different effects in different α regions. In Region 1 (Figure 5), the scattering is almost parallel to the constant energy surface, and thus transit time scattering occurs primarily in α . As α increases, and Landau resonance becomes stronger, and the net scattering yields a resultant single wave characteristic oriented in the radial direction, producing a null in α scattering. For the 300 keV electron, the null occurs at $\alpha_{12} = 30.55^\circ$, and is visible in Figure 4a

as the separatrix between regions 1 and 2. Conversely, in Region 3, the scattering in v_{\perp} is almost perpendicular to the constant energy surface, and thus transit time scattering occurs primarily in E . As α decreases, and Landau resonance becomes stronger, and the net scattering yields a resultant single-wave characteristic oriented parallel to the constant energy surface, going through a null in E scattering. For a 300 keV electron, the null occurs at $\alpha_{23} = 73.55^\circ$, and is visible in Figure 4b as the separatrix between regions 2 and 3.

[18] The time spent by the electron in the wave packet increases dramatically with increasing α_0 and decreasing E_0 . It is instructive to measure the time taken by the particle to traverse the wave packet between the $0.1 B_0^w$ intensity marks ($\lambda \sim -3^\circ$ to 3°), in terms of the wave period ($T_0 = 1/f = 30$ ms.). The normalized transit time map is shown in Figure 6, and indicates that the broad region of nonresonant transit time scattering exhibited in Figures 4c and 4d corresponds to electrons that pass through the wave in less than 2 wave periods. The $4T_0$, $5T_0$, and $8T_0$ contours from Figure 6 are superimposed on Figure 4, and show that the nodes in $D_{\alpha\alpha}$ and D_{EE} essentially coincide with an integer multiple of wave periods traversed by the transit electron (i.e., perfect cancellation in scattering), whereas the antinodes correspond to an additional one-half wave period which remains uncanceled, and thus results in transit time diffusion as described above, albeit far weaker.

[19] In order to separate the resonant from the nonresonant effects, we increase the wave normal angle to $\psi = 89.99^\circ$, such that $v_{\parallel}^{\text{res}} > c$ and no resonant interaction is possible. The remaining scattering is due entirely to transit time diffusion and is shown in Figures 4c and 4d. As expected, the pronounced nulls that were present in the $D_{\alpha\alpha}$ and D_{EE} maps when $\psi = 89^\circ$ due to interference between Landau and transit time diffusion have disappeared in the case when $\psi = 89.99^\circ$, and have been replaced by a broad maximum centered roughly at $E_0 \sim 200$ – 300 keV and $\alpha_0 \sim 50^\circ$ – 60° . The maximum values of the diffusion coefficients are $D_{\alpha\alpha}^{\text{max}}(\psi = 89^\circ) = 3.7 \times 10^{-6} \text{ s}^{-1}$ and $D_{EE}^{\text{max}}(\psi = 89^\circ) = 1.1 \times 10^{-6} \text{ s}^{-1}$, and $D_{\alpha\alpha}^{\text{max}}(\psi = 89.99^\circ) = 7.9 \times 10^{-8} \text{ s}^{-1}$ and $D_{EE}^{\text{max}}(\psi = 89.99^\circ) = 3.9 \times 10^{-7} \text{ s}^{-1}$. While the transit time scattering in α_0 is relatively ineffectual (only $\sim 2\%$ of the Landau resonant scattering), the scattering in E_0 is nevertheless substantial, and is within a factor of 3 of the Landau scattering rate.

[20] The actual importance of transit time energy diffusion relative to resonant (Landau) energy diffusion may be even greater than is indicated by the analysis above. Since the MS wave has a propagation trajectory that “snakes” about the equator, the corresponding wave normal angle varies between a minimum angle, e.g., $\psi = 89^\circ$ at the equator, and $\psi = 90^\circ$ at the wave turning point. Thus, MS waves only have the optimum wave normal distribution ($\psi \sim 89^\circ$) for a relatively short portion of the wave trajectory, near the equator, where they are able to Landau resonate with ~ 0.1 – 1 MeV electrons. As soon as the MS wave propagates away from the equator, its wave normal angle increases, and the resonant energy increases rapidly. Similarly, variations in the background cold-plasma density will significantly affect the range of Landau resonant energies that can be affected by the MS wave. In contrast, transit time diffusion is relatively insensitive to the precise wave normal distribution and is able to

scatter electrons over the entire latitudinal extent of the waves.

5. Conclusions

[21] A test particle approach was used to model the scattering of energetic electrons traversing an equatorially confined magnetosonic wave packet. The parameters of the wave were chosen to match those of Horne *et al.* [2007] as closely as possible and it was shown that to high accuracy, the scattering was linear though this was not necessarily to be expected at the outset. As a result, equivalent diffusion coefficients were calculated from the test particle results as a function of initial energy, and pitch angle. Our results show that:

[22] 1. Diffusion due to Landau-resonant interactions occurred in a similar $E - \alpha$ region, and with roughly similar magnitudes to the predictions of quasilinear theory.

[23] 2. An additional, weaker scattering mechanism appeared, that we called “transit time diffusion.” This resulted from the relatively short time that the energetic particle spent in the wave packet (typically less than 1 wave period) due to the confinement of the wave power to the equatorial region, the large wave-normal angle of the wave, and the low wave frequency.

[24] 3. The orientation of the single-wave characteristic in velocity-space for transit time diffusion was shown to be perpendicular to that of the Landau resonance, resulting in a separation of E and α diffusion into three distinct regions, marked by nulls in either E or α scattering.

[25] 4. When resonant scattering was removed from the energy and pitch angle diffusion maps by choosing an almost perpendicular wave normal angle ($\psi = 89.99^\circ$) which makes the Landau resonance condition impossible to satisfy, it was shown that transit time scattering in pitch angle was relatively ineffectual (~ 50 times weaker than resonant scattering), but transit time scattering in energy remained within a factor of ~ 3 relative to Landau scattering, and in reality could be even more effective due to the variation of the MS wave normal angle as a function of latitude, which tends to reduce Landau resonance, but does not significantly affect transit time scattering.

[26] **Acknowledgments.** This work was supported by NASA grant NNX08AQ88G. We thank Richard B. Horne for constructive discussions.

[27] Robert Lysak thanks Mary Hudson and another reviewer for their assistance in evaluating this paper.

References

- Albert, J. M., and J. Bortnik (2009), Nonlinear interaction of radiation belt electrons with electromagnetic ion cyclotron waves, *Geophys. Res. Lett.*, *36*, L12110, doi:10.1029/2009GL038904.
- Bell, T. F. (1984), The nonlinear gyroresonance interaction between energetic electrons and coherent VLF waves propagating at an arbitrary angle with respect to the Earth’s magnetic field, *J. Geophys. Res.*, *89*(A2), 905–918.
- Boardsen, S. A., D. L. Gallagher, D. A. Gurnett, W. K. Peterson, and J. L. Green (1992), Funnel-shaped low-frequency equatorial waves, *J. Geophys. Res.*, *97*, 14,967–14,976.
- Bortnik, J., U. S. Inan, and T. F. Bell (2006), Temporal signatures of radiation belt electron precipitation induced by lightning-generated MR whistler waves: 1. Methodology, *J. Geophys. Res.*, *111*, A02204, doi:10.1029/2005JA011182.

- Bortnik, J., R. M. Thorne, and U. S. Inan (2008), Nonlinear interaction of energetic electrons with large amplitude chorus, *Geophys. Res. Lett.*, *35*, L21102, doi:10.1029/2008GL035500.
- Denton, R. E., J. Goldstein, and J. D. Menietti (2002), Field line dependence of magnetospheric electron density, *Geophys. Res. Lett.*, *29*(24), 2205, doi:10.1029/2002GL015963.
- Green, J. L., S. Boardsen, L. Garcia, W. W. L. Taylor, S. F. Fung, and B. W. Reinisch (2005), On the origin of whistler mode radiation in the plasmasphere, *J. Geophys. Res.*, *110*, A03201, doi:10.1029/2004JA010495.
- Gurnett, D. A. (1976), Plasma wave interactions with energetic ions near the magnetic equator, *J. Geophys. Res.*, *81*, 2765–2770.
- Horne, R. B., G. V. H. Wheeler, and C. K. St. Alleyne (2000), Proton and electron heating by radially propagating fast magnetosonic waves, *J. Geophys. Res.*, *105*, 27,597–27,610.
- Horne, R. B., R. M. Thorne, S. A. Glauert, N. P. Meredith, D. Pokhotelov, and O. Santolik (2007), Electron acceleration in the Van Allen radiation belts by fast magnetosonic waves, *Geophys. Res. Lett.*, *34*, L17107, doi:10.1029/2007GL030267.
- Jasna, D., U. S. Inan, and T. F. Bell (1992), Precipitation of suprathermal (100 eV) electrons by oblique whistler waves, *Geophys. Res. Lett.*, *19*(16), 1639–1642.
- Kasahara, Y., H. Kenmochi, and I. Kimura (1994), Propagation characteristics of the ELF emissions observed by the satellite Akebono in the magnetic equatorial region, *Radio Sci.*, *29*(4), 751–768.
- Kennel, C. F., and F. Engelmann (1966), Velocity space diffusion from weak plasma turbulence in a magnetic field, *Phys. Fluids*, *9*(12), 2377–2388.
- Laakso, H., H. Junginger, A. Roux, R. Schmidt, and C. de Villedary (1990), Magnetosonic waves above $f_c(H^+)$ at geostationary orbit: GEOS 2 results, *J. Geophys. Res.*, *95*, 10,609–10,621.
- Lauben, D. S., U. S. Inan, and T. F. Bell (2001), Precipitation of radiation belt electrons induced by obliquely propagating lightning-generated whistlers, *J. Geophys. Res.*, *106*(A12), 29,745–29,770.
- Meredith, N. P., R. B. Horne, and R. R. Anderson (2008), Survey of magnetosonic waves and proton ring distributions in the Earth’s inner magnetosphere, *J. Geophys. Res.*, *113*, A06213, doi:10.1029/2007JA012975.
- Nemec, F., O. Santolik, K. Gereova, E. Macusova, Y. de Conchy, and N. Cornilleau-Wehrin (2005), Initial results of a survey of equatorial noise emissions observed by the Cluster spacecraft, *Planet. Space Sci.*, *53*, 291–298.
- Nemec, F., O. Santolik, K. Gereova, E. Macusova, H. Laakso, Y. de Conchy, M. Maksimovic, and N. Cornilleau-Wehrin (2006), Equatorial noise: Statistical study of its localization and the derived number density, *Adv. Space Res.*, *37*, 610–616.
- Omura, Y., Y. Katoh, and D. Summers (2008), Theory and simulation of the generation of whistler-mode chorus, *J. Geophys. Res.*, *113*, A04223, doi:10.1029/2007JA012622.
- Perraut, S., A. Roux, P. Robert, R. Gendrin, J. A. Sauvaud, J. M. Bosqued, G. Kremser, and A. Korth (1982), A systematic study of ULF waves above FH^+ from GEOS 1 and 2 measurements and their relationships with proton ring distributions, *J. Geophys. Res.*, *87*, 6219–6236.
- Pokhotelov, D., F. Lefeuvre, R. B. Horne, and N. Cornilleau-Wehrin (2008), Survey of ELF-VLF plasma waves in the outer radiation belt observed by Cluster STAFF-SA experiment, *Ann. Geophys.*, *26*, 3269–3277.
- Roberts, C. S., and M. Schulz (1968), Bounce resonant scattering of particles trapped in the Earth’s magnetic field, *J. Geophys. Res.*, *73*(23), 7361–7376.
- Russell, C. T., R. E. Holzer, and E. J. Smith (1970), OGO 3 observations of ELF noise in the magnetosphere: The nature of equatorial noise, *J. Geophys. Res.*, *75*, 755–768.
- Santolik, O., J. S. Pickett, D. A. Gurnett, M. Maksimovic, and N. Cornilleau-Wehrin (2002), Spatiotemporal variability and propagation of equatorial noise observed by Cluster, *J. Geophys. Res.*, *107*(A12), 1495, doi:10.1029/2001JA009159.
- Santolik, O., F. Nemec, K. Gereova, E. Macusova, Y. de Conchy, and N. Cornilleau-Wehrin (2004), Systematic analysis of equatorial noise below the lower hybrid frequency, *Ann. Geophys.*, *22*, 2587–2595.
- Stix, T. H. (1992), *Waves in Plasmas*, Springer-Verlag, New York.
- Walker, A. D. M. (1993), *Plasma Waves in the Magnetosphere*, Springer-Verlag, New York.
- Walt, M. (1994), *Introduction to Geomagnetically Trapped Radiation*, Cambridge Univ. Press, Cambridge, U. K.

J. Bortnik and R. M. Thorne, Department of Atmospheric and Oceanic Sciences, University of California, Los Angeles, CA 90095-1565, USA. (jbortnik@gmail.com; rmt@atmos.ucla.edu)